J. Fluid Mech. (1979), *vol.* 90, *part* 2, *pp.* 209–226
Printed in Great Britain

The unsteady pressure field of a ducted impeller

By DAC Q. DANG AND D. H. NORRIE
Department of Mechanical Engineering, University of Calgary, Canada T2N 1N4

(Received 21 November 1977)

Analyses based on a three-dimensional vortex-filament model are presented for the unsteady pressure field generated by a ducted propeller. An oscillating part is identified in the kernels and absolute terms of the governing equations for the harmonic components, allowing two methods to be developed for the solution of the higher harmonics. The first method is exact and is applicable to ducted propellers with practical configurations (small chord-to-diameter ratio) while the second is approximate but more suitable for ducted systems with large chord-to-diameter ratios. The second method was applied to a configuration for which experimental data were available and good agreement was obtained for pressure harmonic amplitudes downstream of the propeller and for phase angles upstream of the propeller.

Special consideration was given to the Kutta–Joukowski condition at the duct trailing edge and a general constraint developed for the doubly coupled governing integral equations.

1. Introduction

Within the last two decades, there has been a resurgence of interest in the ducted or shrouded propeller. Marine application has extended to large tankers as well as to tugs and fishing vessels, whilst aeronautical use has included both short and vertical take-off craft. An increasing number of theoretical and experimental investigations have been reported, a full symposium being devoted in 1973 to the subject of ducted propellers.† A survey of earlier work was published in 1962 (Burnell & Sacks 1962) and both a review of theory (Weissinger & Maass 1968) and a comparison of theory and experiment (Morgan & Caster 1968) were presented in 1968.

Considerable attention has been given to the time-average or 'steady-state' velocity and pressure fields of a ducted propeller but the higher-harmonic components of the flow have been studied less intensively despite their importance for the vibration characteristics of the ship–propulsor combination. The present paper develops procedures for the computation of the higher-harmonic components and gives a comparison between theory and experiment for the case of a long parallel duct.

2. Formulation of the governing equations

The following analysis of the ducted propeller uses the vortex-filament model and the governing-equation formulation of Ordway, Sluyter & Sonnerup (1960). In the original analysis the major variables were non-dimensionalized but for the present

† *Proc. Symp. Ducted Propellers, Nat. Phys. Lab., Teddington, England.* Roy. Inst. Naval Archit., 1973.

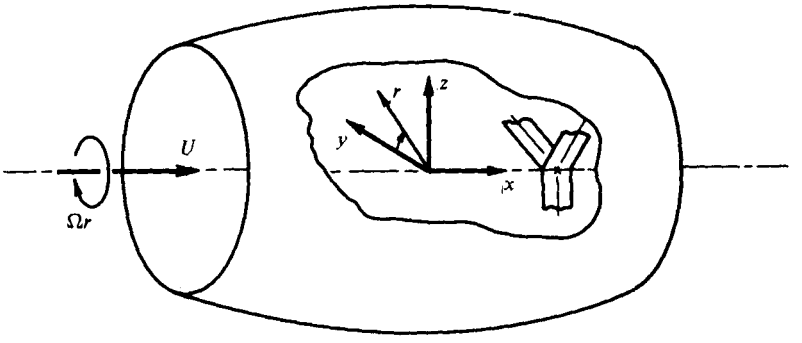

FIGURE 1. Geometry of the ducted propeller.

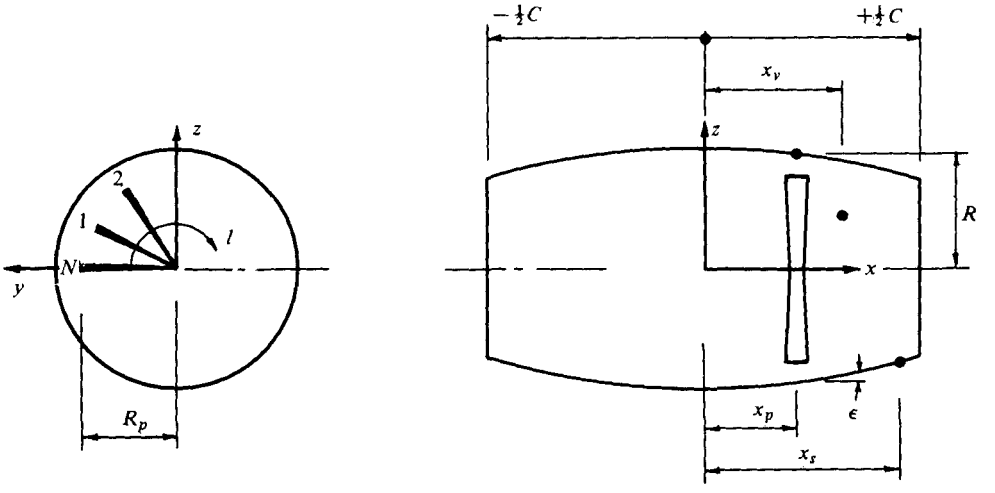

FIGURE 2. Shroud and propeller configuration.

investigation the formulation was reworked to give a normalized representation of parameters and equations. Significant advantages, particularly in integral evaluation, were found with the latter representation. The details of the formulation are given in Dang & Norrie (1975).

The geometry of the ducted propeller is shown in figure 1 and the shroud and propeller configuration in figure 2. The vortex-filament model, shown in figure 3, comprises the following:

(i) bound blade vortices (straight) of strength $\Gamma(r_v)$,

(ii) shed blade vortices (helical) of strength $-\Gamma'(r_v)$,

(iii) bound shroud vortices (ring) of strength $\gamma(x_s, \theta_s, r_s)$,

(iv) shed shroud vortices (helical) of strength $-\partial\gamma/\partial\theta_s$.

The duct is axisymmetric with respect to the oncoming flow of axial velocity U and rotational velocity Ωr. To remove time dependence, body-fixed co-ordinates have been chosen, and since the potential flow is unaffected by shroud rotation, the solution obtained will be mathematically equivalent to that for a translating duct with a rotating propeller in stationary fluid.

Except at a vortex filament, potential flow is assumed throughout. The vortices

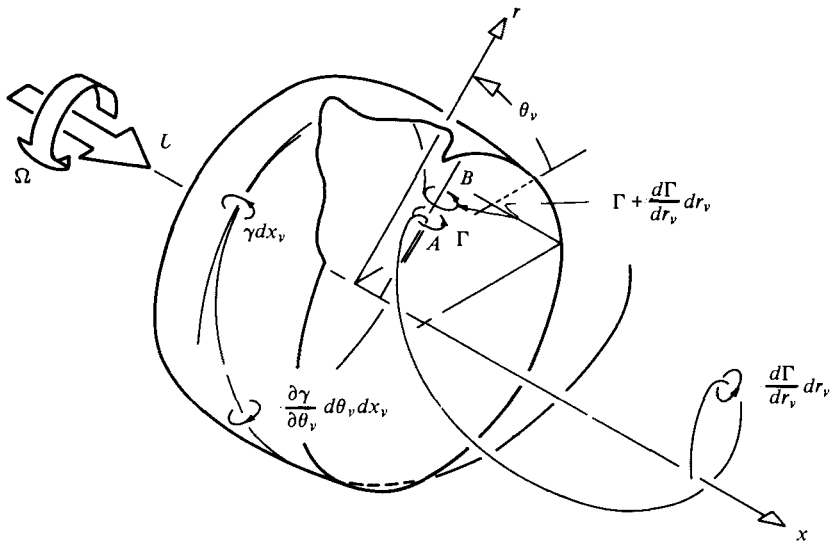

FIGURE 3. Vortex-filament model.

shed from the bound blade and shroud systems are assumed to be carried downstream in helical forms without contraction of the slipstream.

Using the thin-aerofoil approximation, the governing equation is obtained from the condition that the flow is tangential everywhere on the shroud:

$$U\epsilon(x_s) = \mathbf{q}_i(x_s, R, \theta_s).\mathbf{i}_r. \tag{1}$$

The total induced velocity vector $\mathbf{q}_i$ is given by the sum of the induced velocities (at the shroud point (x_s, R, θ_s) being considered) due to the four component vortex systems:

$$\mathbf{q}_i = \mathbf{q}_\Gamma + \mathbf{q}_{\Gamma'} + \mathbf{q}_\gamma + \mathbf{q}_{\gamma'}. \tag{2}$$

The radial components of the induced fields needed in (1) can be found from the Biot–Savart law.

Velocity induced by propeller bound vortices:

$$\mathbf{q}_\Gamma.\mathbf{i}_r = -\frac{\Delta x_p}{4\pi} \sum_{l=1}^{N} \sin\Delta\theta_l \int_0^{R_p} \Gamma(r_v)\, D^{-3}\, dr_v. \tag{3}$$

Velocity induced by propeller shed vortices:

$$\mathbf{q}_{\Gamma'}.\mathbf{i}_r = \frac{1}{4\pi} \sum_{l=1}^{N} \int_0^{R_p} \Gamma'(r_v)\, r_v \int_0^{\infty} \frac{U\sin\Delta\theta_{l\tau} - \Omega\Delta x_{p\tau}\cos\Delta\theta_{l\tau}}{D^3}\, d\tau\, dr_v. \tag{4}$$

Velocity induced by shroud bound vortices:

$$\mathbf{q}_\gamma.\mathbf{i}_r = \frac{R}{4\pi} \int_{-\frac{1}{2}c}^{\frac{1}{2}c} \Delta x_v \int_{-\pi}^{\pi} \gamma D^{-3} \cos\Delta\theta_v\, d\theta_v\, dx_v. \tag{5}$$

Velocity induced by shroud shed vortices:

$$\mathbf{q}_{\gamma'}.\mathbf{i}_r = \frac{R}{4\pi} \int_{-\frac{1}{2}c}^{\frac{1}{2}c} \int_{-\pi}^{\pi} \frac{\partial\gamma}{\partial\theta_v} \int_0^{\infty} [U\sin\Delta\theta_{v\tau} - \Omega\Delta x_{v\tau}\cos\Delta\theta_{v\tau}]\, D^{-3}\, d\tau\, d\theta_v\, dx_v. \tag{6}$$

Substitution of (3)–(6) into (1) yields the general equation for the inverse–direct problem being considered (where it is assumed that the blade circulation and the shroud geometry are specified).

From periodicity considerations, the strength $\gamma(\hat{x}_s, \theta_s)$ of the bound shroud vortices can be expressed as the Fourier expansion

$$\gamma(\hat{x}_s, \theta_s) = U \sum_{m=-\infty}^{\infty} C_m(\hat{x}_s) \exp(imN\theta_s), \tag{7}$$

where the complex Fourier coefficient $C_m(\hat{x}_s)$ for positive and negative harmonic numbers $\pm m$, respectively, is given in terms of cosine and sine coefficients B_m and A_m by

$$2C_{-m}(\hat{x}_s) \equiv B_m(\hat{x}_s) + iA_m(\hat{x}_s), \tag{8}$$

$$2C_{+m}(\hat{x}_s) \equiv B_m(\hat{x}_s) - iA_m(\hat{x}_s). \tag{9}$$

It is also assumed that the radial components of the blade bound and shed induced velocities can be expressed in the following Fourier series:

$$\mathbf{q}_\Gamma . \mathbf{i}_r \equiv \lambda U \sum_{m=-\infty}^{\infty} C_{\Gamma m}(\Delta\hat{x}_p) \exp(imN\theta_s), \tag{10}$$

$$\mathbf{q}_{\Gamma'} . \mathbf{i}_r \equiv \lambda U^r \sum_{m=-\infty}^{\infty} C_{\Gamma' m}(\Delta\hat{x}_p) \exp(imN\theta_s). \tag{11}$$

Substitution of (7), (10) and (11) into the previously obtained general equation and use of the trigonometric integral form of the Legendre function of the second kind and half-integer order yields the governing equation in the form

$$\delta_{0m}\hat{\epsilon}(\hat{x}_s) - C_{\Gamma m}(\Delta\hat{x}_p) - C_{\Gamma' m}(\Delta\hat{x}_p) = \int_{-1}^{1} C_m(\hat{x}_v) [F_{\gamma m}(\Delta\hat{x}_v) + F_{\gamma' m}(\Delta\hat{x}_v)] \, d\hat{x}_v, \tag{12}$$

where $F_{\gamma m}$, $F_{\gamma' m}$, $C_{\Gamma m}$ and $C_{\Gamma' m}$ are given in terms of the Legendre-function combinations S_{mN} and T_{mN} by

$$F_{\gamma m}(\Delta\hat{x}_v) = -\frac{\lambda \Delta\hat{x}_v}{4\pi} S'_{mN}(\tilde{\omega}_1), \tag{13}$$

$$F_{\gamma' m}(\Delta\hat{x}_v) = \frac{imN\lambda}{4\pi} \int_0^\infty \exp(-imN\bar{\tau}) \left[\Delta\hat{x}_{v\tau} S'_{mN}(\tilde{\omega}_2) - \frac{iJ\mu}{\lambda} T'_{mN}(\tilde{\omega}_2) \right] d\bar{\tau}, \tag{14}$$

$$C_{\Gamma m}(\Delta\hat{x}_p) = \frac{i\mu^{\frac{1}{2}} N \Delta\hat{x}_p}{8\pi^2} \int_0^1 \frac{\hat{\Gamma}(\hat{r}_v)}{\hat{r}_v^{\frac{3}{2}}} T'_{mN}(\tilde{\omega}_3) \, d\hat{r}_v, \tag{15}$$

$$C_{\Gamma' m}(\Delta\hat{x}_p) = \frac{\mu^{\frac{1}{2}} N}{8\pi^2} \int_0^1 \frac{\hat{\Gamma}(\hat{r}_v)}{\hat{r}_v^{\frac{1}{2}}} \int_0^\infty \exp(-imN\bar{\tau}) \left[\Delta\hat{x}_p S'_{mN}(\tilde{\omega}_4) - \frac{iJ\mu}{\lambda} T'_{mN}(\tilde{\omega}_4) \right] d\bar{\tau} \, d\hat{r}_v. \tag{16}$$

The Legendre combinations are defined by

$$S_{mN}(\tilde{\omega}) \equiv Q_{mN+\frac{1}{2}}(\tilde{\omega}) + Q_{mN-\frac{3}{2}}(\tilde{\omega}), \tag{17}$$

$$T_{mN}(\tilde{\omega}) \equiv Q_{mN+\frac{1}{2}}(\tilde{\omega}) - Q_{mN-\frac{3}{2}}(\tilde{\omega}), \tag{18}$$

where $Q_{mN+\frac{1}{2}}$ and $Q_{mN-\frac{3}{2}}$ are Legendre functions of the second kind and half-integer order and the arguments $\tilde{\omega}_1$, $\tilde{\omega}_2$, $\tilde{\omega}_3$ and $\tilde{\omega}_4$ are given by

$$\tilde{\omega}_1 \equiv 1 + \tfrac{1}{2}\lambda^2 \Delta\hat{x}_v^2, \quad \tilde{\omega}_2 \equiv 1 + \tfrac{1}{2}\lambda^2 \Delta\hat{x}_{v\tau}^2, \tag{19), (20}$$

$$\tilde{\omega}_3 \equiv \frac{1+\lambda^2\Delta\hat{x}_p^2+[1-\mu\hat{r}_v]^2}{2\mu\hat{r}_v}, \quad \tilde{\omega}_4 \equiv 1+\frac{\lambda^2\Delta\hat{x}_{p_T}^2+[1-\mu\hat{r}_v]^2}{2\mu\hat{r}_v}. \tag{21),(22}$$

The general governing equation (12) applies to all harmonic numbers of the doubly infinite Fourier expansion of the shroud bound vortex strength and includes both the real and the imaginary terms of the various vortices' contributions. Separation of this general equation into real and imaginary parts produces an infinite set of coupled pairs of integral equations in the unknowns A_m and B_m covering all harmonic numbers m. Following this decomposition, substitution of various Legendre recursion relationships and some manipulation yield doubly coupled integral equations (for all m) of the form

$$2\delta_{0m}\hat{e}(\hat{x}_s)-B_{\Gamma' m}(\Delta\hat{x}_p) = \hat{\sigma}\int_{-1}^{1} A_m(\hat{x}_v)\,K_m(\Delta\hat{x}_v)\,d\hat{x}_v - \int_{-1}^{1} B_m(\hat{x}_v)\,K'_m(\Delta\hat{x}_v)\,d\hat{x}_v, \tag{23}$$

$$A_{\Gamma m}(\Delta\hat{x}_p)+A_{\Gamma' m}(\Delta\hat{x}_p) = \hat{\sigma}\int_{-1}^{1} B_m(\hat{x}_v)\,K_m(\Delta\hat{x}_v)\,d\hat{x}_v + \int_{-1}^{1} A_m(\hat{x}_v)\,K'_m(\Delta\hat{x}_v)\,d\hat{x}_v, \tag{24}$$

where $B_{\Gamma' m}$, $A_{\Gamma m}$, $A_{\Gamma' m}$, K_m and K'_m are given by

$$B_{\Gamma' m}(\Delta\hat{x}_p) = \frac{\mu^{\frac{1}{2}}N}{4\pi^2 J\lambda}\int_0^1 \hat{\Gamma}'(\hat{r}_v)\,\hat{r}_v^{\frac{1}{2}}\,[S_{mN}(\tilde{\omega}_3)-g_{mN}(\Delta\hat{x}_p,\hat{r}_v)]\,d\hat{r}_v, \tag{25}$$

$$A_{\Gamma m}(\Delta\hat{x}_p) = -\frac{\mu^{\frac{1}{2}}mN^2\Delta\hat{x}_p}{2\pi^2}\int_0^1 \frac{\hat{\Gamma}(\hat{r}_v)}{\hat{r}_v^{\frac{3}{2}}}\,Q_{mN-\frac{1}{2}}(\tilde{\omega}_3)\,d\hat{r}_v, \tag{26}$$

$$A_{\Gamma' m}(\Delta\hat{x}_p) = \frac{\mu^{\frac{1}{2}}N}{4\pi^2 J\lambda}\int_0^1 \hat{\Gamma}'(\hat{r}_v)\,\hat{r}_v^{\frac{1}{2}}\,h_{mN}(\Delta\hat{x}_p,\hat{r}_v)\,d\hat{r}_v, \tag{27}$$

$$K_m(\Delta\hat{x}_v) = \frac{1}{4\pi\lambda}\left[S_{mN}(\tilde{\omega}_1)-g_{mN}\left(\Delta\hat{x}_v,\frac{1}{\mu}\right)\right], \tag{28}$$

$$K'_m(\Delta\hat{x}_v) = \frac{1}{4\pi\lambda}\left[\lambda^2\Delta\hat{x}_v S'_{mN}(\tilde{\omega}_1)-\hat{\sigma}h_{mN}\left(\Delta\hat{x}_v,\frac{1}{\mu}\right)\right]. \tag{29}$$

The parameters h_{mN} and g_{mN} are Fourier integrals defined by

$$h_{mN}(\Delta\hat{x}_p,\hat{r}_v) \equiv mN\int_0^\infty \left[S_{mN}(\tilde{\omega}_4)+\frac{2J^2\mu}{\hat{r}_v}\,Q_{mN-\frac{1}{2}}(\tilde{\omega}_4)\cos mN\bar{\tau}\,d\bar{\tau}, \tag{30}$$

$$g_{mN}(\Delta\hat{x}_p,\hat{r}_v) \equiv mN\int_0^\infty \left[S_{mN}(\tilde{\omega}_4)+\frac{2J^2\mu}{\hat{r}_v}\,Q_{mN-\frac{1}{2}}(\tilde{\omega}_4)\right]\sin mN\bar{\tau}\,d\bar{\tau}. \tag{31}$$

The governing equations for the inverse–direct problem are thus the doubly coupled integral equations (23) and (24). The unknowns A_m and B_m, for each harmonic number m, are the imaginary and real parts of the coefficient C_m of the Fourier expansion of the shroud vorticity γ.

3. The steady-state solution

For $m = 0$, (24) vanishes and the steady-state solution is the zeroth-harmonic form of (23). This is a Fredholm integral equation of the first kind in which the kernel exhibits a weak Cauchy singularity. Solution procedures for this equation are described by Ordway *et al.* (1960), Dang (1972, 1975*a*, *b*), Dang & Norrie (1975) and Ordway & Greenberg (1961).

4. The higher-harmonic solution

4.1. *The parameters of the higher-harmonic solution*

The higher-harmonic solutions to the ducted-propeller problem are much more complex than those for the zeroth harmonic, requiring solutions to the doubly coupled Fredholm equations (23) and (24). Ordway *et al.* proposed two methods for the higher harmonics but did not apply either of these to the computation of a particular configuration. Moreover, the possibility of oscillation in the kernel was not considered in these methods and their applicability can be questioned since it was found in the present investigation that such an oscillating part does exist. The kernels thus comprise regular, singular and oscillating parts. It should be noted that, although it appears that the oscillating part has not been previously reported, its existence determines the practicality and accuracy of the several approximate methods developed for the solution of the coupled integral equations, particularly in the case of large λ (or, specifically, large $\hat{\sigma}$).

Before the governing equations (23) and (24) can be solved, the absolute terms $B_{\Gamma' m}(\Delta\hat{x}_p)$, $A_{\Gamma m}(\Delta\hat{x}_p)$ and $A_{\Gamma' m}(\Delta\hat{x}_p)$ and the kernel $K_m(\Delta\hat{x}_v)$ and its derivative $K'_m(\Delta\hat{x}_v)$ must be evaluated. From (25)–(29), it is seen that these five parameters depend on the Legendre functions $Q_{mN-\frac{1}{2}}$ and S_{mN} and the Fourier integrals h_{mN} and g_{mN}, with the absolute terms additionally dependent on the specified propeller circulation distribution Γ.

4.2. *Decomposition into regular, singular and oscillating parts*

Consideration of the Fourier integrals h_{mN} and g_{mN} given in (30) and (31) shows (Dang 1974) that they can each be decomposed into a regular and an oscillating part. The regular parts of h_{mN} and g_{mN} are respectively odd and even about $\Delta\hat{x}_p = 0$ and the oscillating parts exist only for $\Delta\hat{x}_p > 0$. Hence for $\Delta\hat{x}_p > 0$,

$$h_{mN}(\Delta\hat{x}_p, \hat{r}_v) = h_{mN_R}(\Delta\hat{x}_p, \hat{r}_v) + h_{mN_O}(\Delta\hat{x}_p, \hat{r}_v), \tag{32}$$

$$g_{mN}(\Delta\hat{x}_p, \hat{r}_v) = g_{mN_R}(\Delta\hat{x}_p, \hat{r}_v) + g_{mN_O}(\Delta\hat{x}_p, \hat{r}_v), \tag{33}$$

where the regular parts h_{mN_R} and g_{mN_R} are given by

$$h_{mN_R}(\Delta\hat{x}_p, \hat{r}_v) = -h_{mN}(-\Delta\hat{x}_p, \hat{r}_v), \quad g_{mN_R}(\Delta\hat{x}_p, \hat{r}_v) = g_{mN}(-\Delta\hat{x}_p, \hat{r}_v) \tag{34), (35}$$

and the oscillating parts h_{mN_O} and g_{mN_O} are given by

$$h_{mN_O}(\Delta\hat{x}_p, \hat{r}_v) = 2H_{mN}(\hat{r}_v)\cos(\hat{\sigma}\Delta\hat{x}_p), \quad g_{mN_O}(\Delta\hat{x}_p, \hat{r}_v) = 2H_{mN}(\hat{r}_v)\sin(\hat{\sigma}\Delta\hat{x}_p). \tag{36), (37}$$

The functions H_{mN} and G_{mN} in (36) and (37) are defined by

$$\begin{matrix} H_{mN} \\ G_{mN} \end{matrix}(\hat{r}_v) \equiv mN \int_0^\infty \left[S_{mN}(\tilde{\omega}_4^*) + \frac{2J^2\mu}{\hat{r}_v} Q_{mN-\frac{1}{2}}(\tilde{\omega}_4^*) \right] \begin{matrix} \cos \\ \sin \end{matrix} mN\bar{\tau}\, d\bar{\tau}, \tag{38}$$

where $\tilde{\omega}_4^*$ is $\tilde{\omega}_4$ for the case $\Delta\hat{x}_p = 0$.

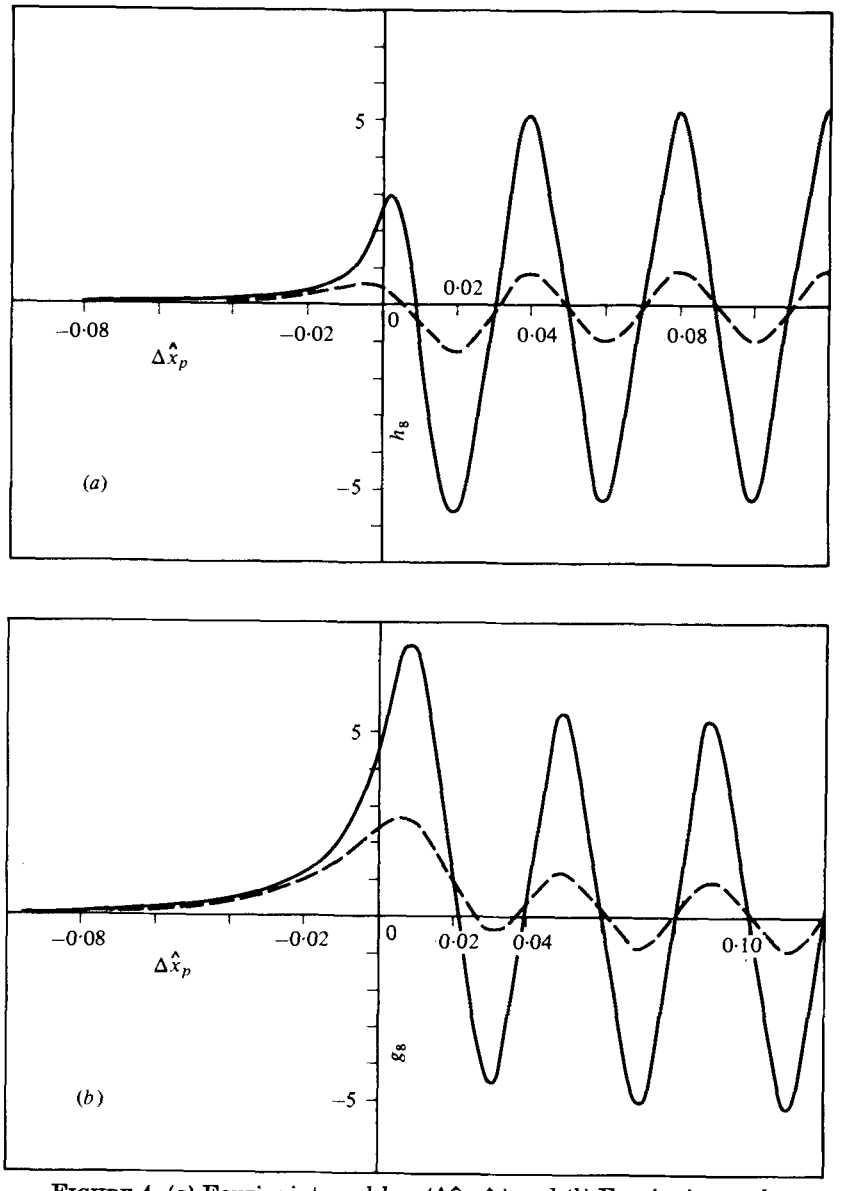

FIGURE 4. (*a*) Fourier integral $h_{mM}(\Delta\hat{x}_p, \hat{r}_v)$ and (*b*) Fourier integral $g_{mN}(\Delta\hat{x}_p, \hat{r}_v)$; $m = 2$. ——, $\hat{r}_v = 1{\cdot}00$; - - - -, $\hat{r}_v = 0{\cdot}95$.

The kernels $K_m(\Delta\hat{x}_v)$ and $K'_m(\Delta\hat{x}_v)$ of the governing equations, because of their dependence on g_{mN} and h_{mN} respectively, also contain an oscillating part, in this case for $\Delta\hat{x}_v > 0$ (since $\Delta\hat{x}_v$ is here the argument for g_{mN} and h_{mN}). These oscillating parts are

$$K_{m_O}(\Delta\hat{x}_v) = -\frac{1}{2\pi\lambda} H_{mN}\left(\frac{1}{\mu}\right) \sin(\hat{\sigma}\Delta\hat{x}_v), \tag{39}$$

$$K'_{m_O}(\Delta\hat{x}_v) = -\frac{\hat{\sigma}}{2\pi\lambda} H_{mN}\left(\frac{1}{\mu}\right) \cos(\hat{\sigma}\Delta\hat{x}_v), \tag{40}$$

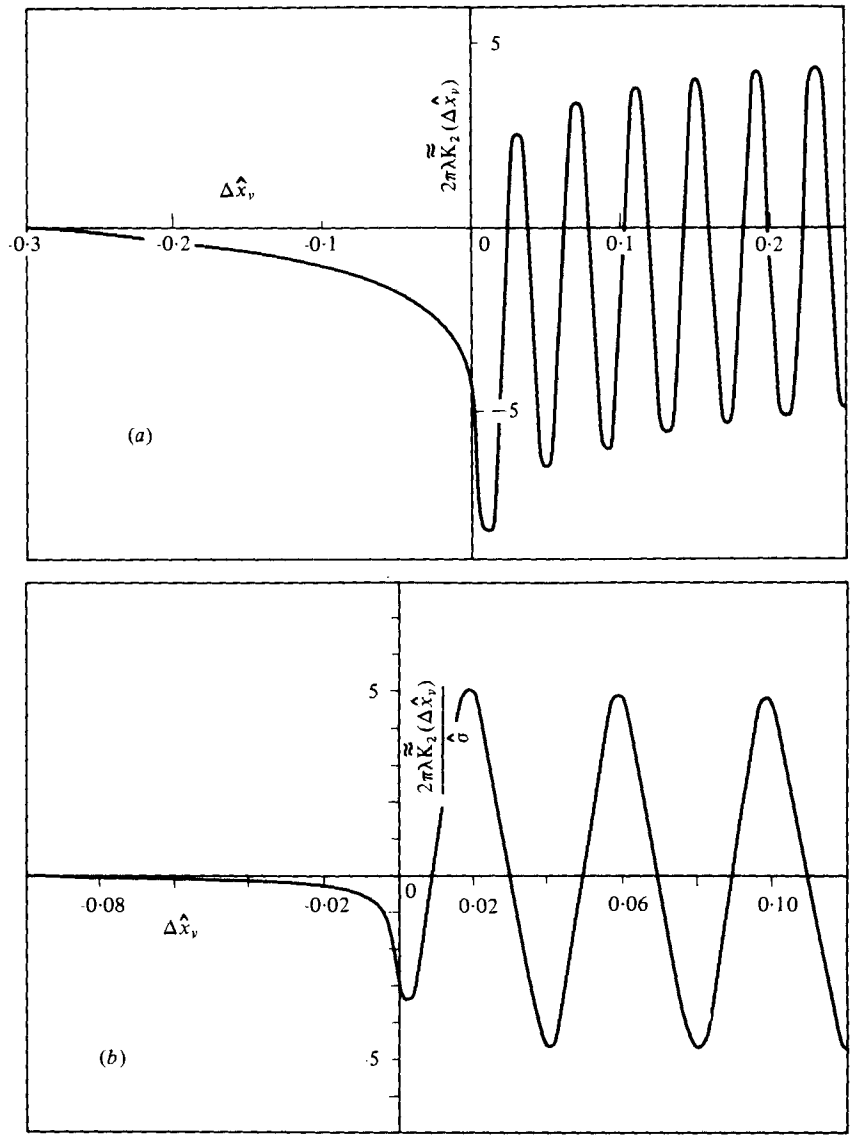

FIGURE 5. 'Regular' part of (*a*) the kernel $K_m(\Delta\hat{x}_v)$ and (*b*) the kernel $K'_m(\Delta\hat{x}_v)$; $m = 2$.

where $H_{mN}(1/\mu)$ and $G_{mN}(1/\mu)$ are given by

$$\begin{matrix} H_{mN} \\ G_{mN} \end{matrix}\left(\frac{1}{\mu}\right) = \int_0^\infty \left[S_{mN}(\tilde{\omega}_2^*) + 2J^2\mu^2 Q_{mN-\frac{1}{2}}(\tilde{\omega}_2^*)\right] \begin{matrix} \cos \\ \sin \end{matrix} mN\bar{\tau}\, d\bar{\tau}, \tag{41}$$

with

$$\tilde{\omega}_2^* = 1 + \tfrac{1}{2}J^2\mu^2\bar{\tau}^2. \tag{42}$$

The kernels K_m and K'_m have logarithmic and Cauchy singularities at $\Delta\hat{x}_v = 0$; thus the singular parts of these kernels are

$$K_{mS} = -\frac{1}{4\pi\lambda}\ln\frac{\lambda^2\Delta\hat{x}_v^2}{2}, \quad K'_{mS} = -\frac{1}{2\pi\lambda\Delta\hat{x}_v}. \tag{43), (44}$$

Subtraction of the oscillating and singular parts from the kernels allows the (true) regular parts to be obtained.

4.3. *Evaluation of the parameters*

Using the quarter-period calculation described by Dang (1973), the Fourier integrals $h_{mN}(\Delta\hat{x}_p, \hat{r}_v)$ and $g_{mN}(\Delta\hat{x}_p, \hat{r}_v)$ can be computed for all $\Delta\hat{x}_p$ and $\hat{r}_v$, the case $\hat{r}_v = 1/\mu$ (duct surface) requiring special attention at $\bar{\tau} = 0$. The general form of these integrals is shown in figures 4(*a*) and (*b*), where h_{mN} and g_{mN} are given for the case of $m = 2$. The oscillatory part for $\Delta\hat{x}_p > 0$ may be clearly seen.

The kernels K_m and K'_m can be computed directly from (28) and (29) using the previously determined values for h_{mN} and g_{mN} together with direct calculation of the Legendre functions. For $m = 2$, the kernels K_m and K'_m are shown in figures 5(*a*) and (*b*) in terms of their 'regular parts' (true regular + oscillating parts).

4.4. *The characteristics of the governing equations*

For the ducted-propeller problem, the governing equations for the higher-harmonic components are (23) and (24), as shown previously. These are Fredholm-type doubly coupled integral equations of the form

$$\sigma_1 \int_{-1}^{1} f(x)\, K(y-x)\, dx + \int_{1}^{1} g(x)\, K'(y-x)\, dx = \Phi(y), \tag{45}$$

$$\sigma_2 \int_{-1}^{1} g(x)\, K(y-x)\, dx + \int_{-1}^{1} f(x)\, K'(y-x)\, dx = \Psi(y), \tag{46}$$

in which the coupling is due to the kernel $K(y-x)$ and its derivative $K'(y-x)$. The standard methods for solving these doubly coupled integral equations are not suited to the characteristics of the kernels and absolute terms in the present case and it was necessary to develop a new solution procedure. The geometric expansion method for the solution of a singular integral equation was outlined in Dang & Norrie (1975; see also Dang 1974, 1975). The method can be extended to doubly coupled integral equations, when it becomes based on a Chebyshev series expansion of the unknowns and a geometric expansion of the regular part of each kernel. In the following, the application of the method to (45) and (46) is briefly outlined. A more detailed explanation has been given by Dang (1974).

4.5. *Homogeneous and particular solutions*

The presence of the Cauchy singularity and the coupling between the governing equations (45) and (46) through the kernels determines the existence of homogeneous solutions f_H and g_H satisfying

$$\sigma_1 \int_{1}^{1} f_H(x)\, K(y-x)\, dx + \int_{-1}^{1} g_H(x)\, K'(y-x)\, dx = 0, \tag{47}$$

$$\sigma_2 \int_{-1}^{1} g_H(x)\, K(y-x)\, dx + \int_{-1}^{1} f_H(x)\, K'(y-x)\, dx = 0. \tag{48}$$

If f_p and g_p denote the particular or inhomogeneous solutions of (45) and (46) the general solutions of these equations are given by

$$f(x) = A_H f_H(x) + f_p(x), \tag{49}$$

$$g(x) = B_H g_H(x) + g_p(x), \tag{50}$$

where A_H and B_H are constants determined by the constraints on the problem. As will be shown subsequently, in the case of the ducted propeller these constants are fixed by the Kutta–Joukowski condition on the shroud.

For the particular solution, a perturbation method has been developed (Dang 1972), but unfortunately the homogeneous solution cannot be obtained readily in this way. The geometric expansion method has therefore been used to determine both the particular and the homogeneous solutions. The perturbation method, however, shows that if a Chebyshev series approximation is adopted the homogeneous solutions will have the following form:

$$f_H(x) \cong \frac{A(1-x)}{\pi(1-x^2)^{\frac{1}{2}}} + \sum_{n=0}^{N} a_{H_n} T_n(x), \tag{51}$$

$$g_H(x) \cong \frac{B(1-x)}{\pi(1-x^2)^{\frac{1}{2}}} + \sum_{n=0}^{N} b_{H_n} T_n(x), \tag{52}$$

where the coefficients A and B are given by

$$A = -2/3\sigma_1 q \log 2, \quad B = -2/3\sigma_2 q \log 2. \tag{53), (54}$$

Similarly, the particular solutions have the forms

$$f_p(x) \cong \frac{A_p(1-x)}{\pi(1-x^2)^{\frac{1}{2}}} + \sum_{n=0}^{N} a_n T_n(x), \tag{55}$$

$$g_p(x) \cong \frac{B_p(1-x)}{\pi(1-x^2)^{\frac{1}{2}}} + \sum_{n=0}^{N} b_n T_n(x), \tag{56}$$

where the coefficients A_p and B_p should be chosen as

$$A_p = \Phi(0)\, A, \quad B_p = \Psi(0)\, B. \tag{57), (58}$$

4.6. *The geometric expansion method*

Using the polynomial expansions

$$\bar{K}(y-x) \cong \sum_{m=0}^{M} p_m [y-x]^m, \quad \bar{K}'(y-x) \cong \sum_{m=0}^{M} m p_m [y-x]^{m-1} \tag{59), (60}$$

for the regular parts of the kernels, together with the previously given approximations for the unknown functions [(51) and (52) or (55) and (56)], yields equations of the following form to be solved for both the homogeneous and the particular solutions:

$$\Phi_e(y) \cong \sigma_1 \sum_{n=0}^{N} a_n \mathscr{P}_n(y) + \sum_{n=0}^{N} b_n \mathscr{Q}_n(y), \tag{61}$$

$$\Psi_e(y) \cong \sigma_2 \sum_{n=0}^{N} b_n \mathscr{P}_n(y) + \sum_{n=0}^{N} a_n \mathscr{Q}_n(y). \tag{62}$$

The functions $\mathscr{P}_n$ and $\mathscr{Q}_n$ can be shown to be given by (Dang 1974)

$$\mathscr{P}_n(y) \equiv qH_n(y) - \frac{q}{2}\log 2 T_n + \sum_{m=0}^{M} p_m \epsilon_n^m(y) + A_0[\sin\beta y\, \mathscr{C}_n(\beta, y) - \cos\beta y\, \mathscr{S}_n(\beta, y)], \tag{63}$$

$$\mathscr{Q}_n(y) \equiv q\mathscr{I}_n(y) + \sum_{m=0}^{M} m p_m \epsilon_n^{m-1}(y) + A_0\beta[\cos\beta y\, \mathscr{C}_n(\beta, y) + \sin\beta y\, \mathscr{S}_n(\beta, y)], \tag{64}$$

where the Chebyshev Fourier integrals $\mathscr{C}_n$ and $\mathscr{S}_n$ are defined by

$$\mathscr{C}_n(\beta, y) \equiv \int_{-1}^{y} T_n(x) \cos \beta x \, dx, \quad \mathscr{S}_n(\beta, y) \equiv \int_{-1}^{y} T_n(x) \sin \beta x \, dx. \quad (65), (66)$$

The special Chebyshev integrals $\mathscr{H}_n$, Υ_n, $\mathscr{I}_n$ and ϵ_n^m are given respectively by

$$\mathscr{H}_n(y) \equiv \int_{-1}^{1} T_n(x) \log (y-x) \, dx, \quad \Upsilon_n \equiv \int_{-1}^{1} T_n(x) \, dx, \quad (67), (68)$$

$$\mathscr{I}_n(y) \equiv \int_{-1}^{1} \frac{T_n(x)}{y-x} dx, \quad \epsilon_n^m(y) \equiv \int_{-1}^{1} T_n(x) (y-x)^m dx. \quad (69), (70)$$

For the homogeneous solutions, the 'effective absolute terms' Φ_e and Ψ_e of (61) and (62) can be shown to be

$$\Phi_{eH}(y) \equiv -\Big\{1 + \sigma_1 Aqy + \sigma_1 A \sum_{m=0}^{M} p_m[(1-y) Y_m(y) + Y_{m+1}(y) + Bq + B \sum_{m=0}^{M} m p_m[(1-y) Y_{m-1}(y) + Y_m(y)]\Big\}, \quad (71)$$

$$\Psi_{eH}(y) \equiv -\Big\{1 + \sigma_2 Bqy + \sigma_2 B \sum_{m=0}^{M} p_m[(1-y) Y_m(y) + Y_{m+1}(y)] + Aq + A \sum_{m=0}^{M} m p_m[(1-y) Y_{m-1}(y) + Y_m(y)]\Big\}, \quad (72)$$

whereas, for the particular solutions, Φ_e and Ψ_e are given by

$$\Phi_{ep}(y) \equiv \Phi(y) + \Phi(0) \, \Phi_{eH}(y), \quad \Psi_{ep}(y) \equiv \Psi(y) + \Psi(0) \, \Psi_{eH}(y). \quad (73), (74)$$

The function Y_m needed for both solutions is defined by

$$Y_m(y) \equiv \frac{1}{\pi} \int_{-1}^{1} \frac{(y-x)^m}{(1-x^2)^{\frac{1}{2}}} dx. \quad (75)$$

Applying N-term collocation to the pair of equations (61) and (62) transforms these to the following pair of matrix equations:

$$\mathbf{\Phi}_e = \sigma_1 \mathbf{P}\mathbf{a} + \mathbf{Q}\mathbf{b}, \quad \mathbf{\Psi}_e = \sigma_2 \mathbf{P}\mathbf{b} + \mathbf{Q}\mathbf{a}. \quad (76), (77)$$

The vector $\mathbf{a}$ lists the N unknown coefficients a, the vector $\mathbf{b}$ similarly lists the N unknown coefficients b, and the various other matrices are derived by using N values of y.

If all inverses exist, the solution for the a and b coefficients is obtained from

$$\mathbf{a} = \mathbf{R}^{-1}(\sigma_2 \mathbf{Q}^{-1} \mathbf{\Phi}_e - \mathbf{P}^{-1} \mathbf{\Psi}_e), \quad \mathbf{b} = \mathbf{R}^{-1}(\sigma_1 \mathbf{Q}^{-1} \mathbf{\Psi}_e - \mathbf{P}^{-1} \mathbf{\Phi}_e), \quad (78), (79)$$

where

$$\mathbf{R} = \sigma_1 \sigma_2 (\mathbf{Q}^{-1}\mathbf{P} - \mathbf{P}^{-1}\mathbf{Q}). \quad (80)$$

4.7. *The Kutta–Joukowski condition*

In the vortex model representing the ducted propeller the stagnation point is assumed to be at the trailing edge of the shroud both for the total flow field and for each of the harmonic flow components. The constraint on the governing equations (45) and (46) is therefore

$$\lim_{x \to 1} \{f(x), g(x)\} = 0. \quad (81)$$

Using this relation to determine the constants A_H and B_H in (49) and (50) yields the complete solution to the governing equations in the form

$$f(x) \cong (A_p + D_A A)\frac{1-x}{\pi(1-x^2)^{\frac{1}{2}}} + \sum_{n=0}^{N} [a_n + D_A a_{H_n}] T_n(x), \tag{82}$$

$$g(x) \cong (B_p + D_B B)\frac{1-x}{\pi(1-x^2)^{\frac{1}{2}}} + \sum_{n=0}^{N} [b_n + D_B b_{H_n}] T_n(x), \tag{83}$$

where D_A and D_B are given by

$$D_A = -\sum_{n=0}^{N} a_n \Big/ \sum_{n=0}^{N} a_{H_n}, \qquad D_B = -\sum_{n=0}^{N} b_n \Big/ \sum_{n=0}^{N} b_{H_n}. \tag{84), (85}$$

Since the constants A, B, A_p and B_p can be obtained from (53), (54), (57) and (58) and the a and b coefficients from (78) and (79) for both the homogeneous and the particular solutions, the previously unknown functions $f(x)$ and $g(x)$ are now completely and uniquely determined.

4.8. *Limiting conditions*

The procedure outlined for solution of doubly coupled integral equations of the form of (45) and (46) can in principle be used for any such equation set. In practice, however, it has been found that with the accuracy possible with the available computer (CDC 6400, single precision) the method breaks down if (i) the amplitude of the oscillating part for any parameter is large in comparison with the regular part and (ii) the period of oscillation is 'small'. As the amplitude of the oscillating part increases and the period decreases, the number of collocation points must be increased if the unknowns are to be adequately represented and the resulting increase in error in the matrix calculation is what finally causes the procedure to break down.

Thus, although the method is suitable for ducted propellers where the oscillating part is small and of large period (or where the error accumulation can be circumvented by a very large computational capability) it was not applicable to a particular ducted propeller (the 'Hale configuration') for which experimental results were available. For this unit, both the amplitude of the oscillating part was large and the period was small so the alternative procedure described in the next section was devised to solve the governing equations (45) and (46).

5. The higher-harmonic solution when the oscillating part is dominant

5.1. *Relative influence of the singular, regular and oscillating parts*

For the Hale configuration, preliminary computation showed that the oscillating part was dominant in the kernels and the absolute terms beyond a short distance downstream from the propeller. The kernel $K_m(\Delta\hat{x}_v)$ represents the imaginary part of the influence of the shroud shed vortices, whilst its derivative $K'_m(\Delta\hat{x}_v)$ derives from the real part of the influence of all the shroud vortices (both shed and bound). Thus, far away from the vortex point, i.e. $\Delta\hat{x}_v$ large, the influence of the true regular part (especially in the case of $K'_m(\Delta\hat{x}_v)$, where the true regular part relates to the shroud bound vortices) will tend to be smaller than that of the oscillating part due to the helical shed vortices. Examination of preliminary results showed that, in the case of the kernel $K_1(\Delta\hat{x}_v)$, by $\Delta\hat{x}_v = 0{\cdot}10$ this influence has already decreased to about 10 %

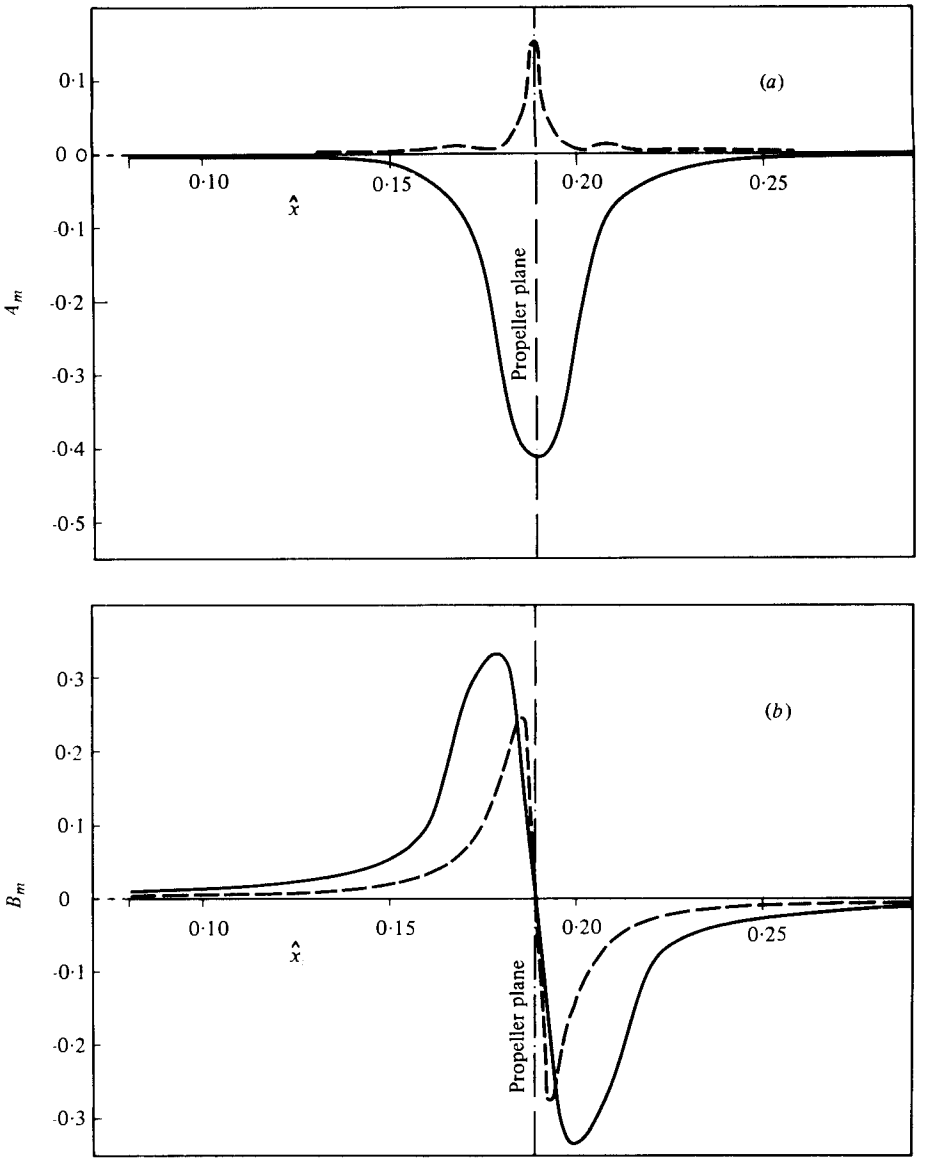

FIGURE 6. Solution of the general governing equations; $J_I = 0{\cdot}74$.
(*a*) $A_m(\hat{x}_s)$. (*b*) $B_m(\hat{x}_s)$. ——, $m = 1$; - - -, $m = 2$.

of that due to the shed vortices. A similar conclusion can be drawn for $K_2(\Delta\hat{x}_v)$ from figure 5 (*a*). The influence of the singular part of the kernel can also be seen to decrease with distance downstream. The regular part of each absolute term similarly decreases with distance downstream.

For the Hale configuration, therefore, since the oscillating part is dominant in the downstream region except near the propeller plane, it can be assumed as a first approximation that the regular part of the absolute terms and the regular and singular parts of the kernels are negligible. As a second approximation, the regular part of the absolute terms can be retained but the regular and singular parts of the kernels still

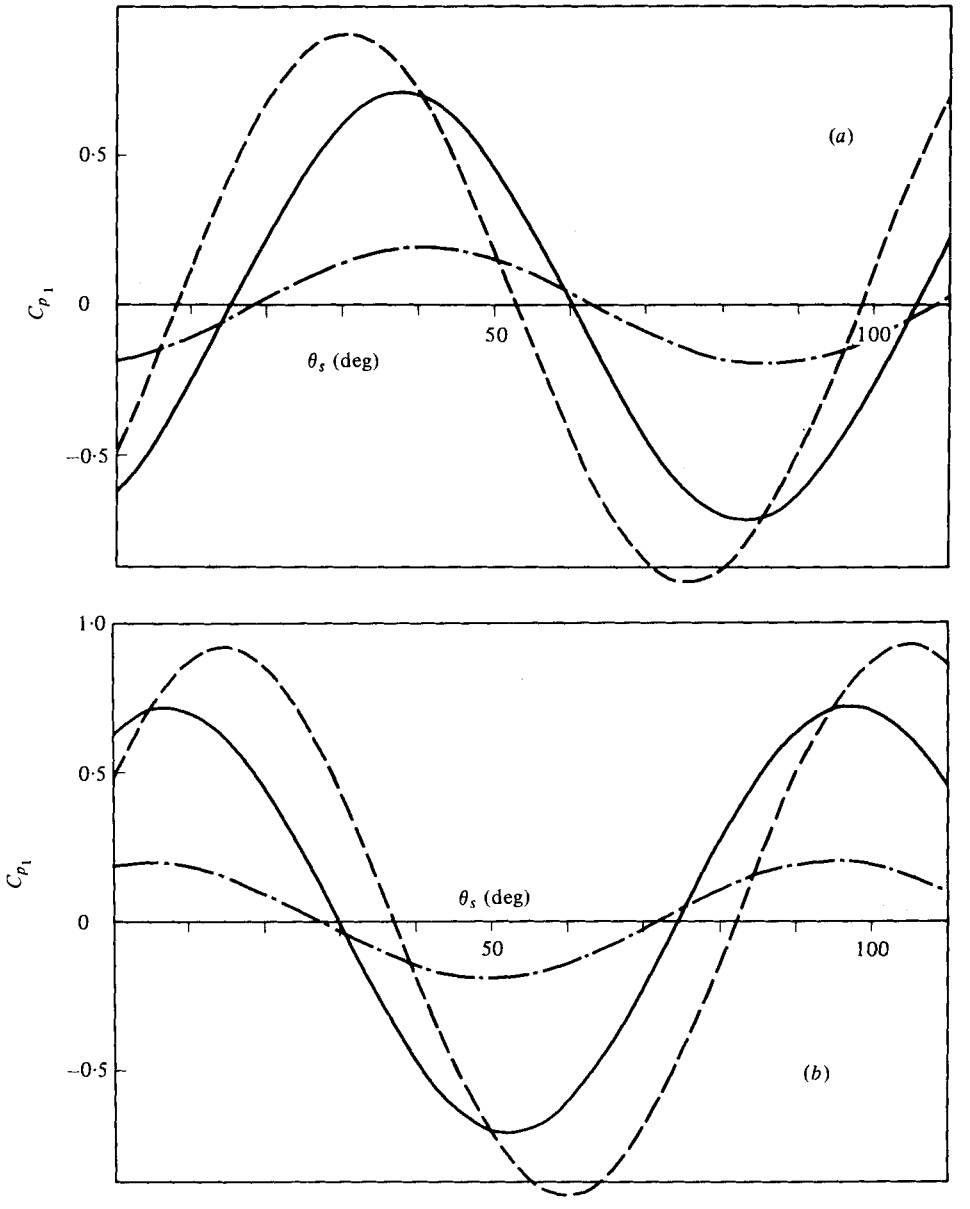

FIGURE 7. Coefficient of harmonic pressure C_{p_m}; $m = 1$. (*a*) Upstream positions. (*b*) Downstream positions. —·—, $\hat{x}_s = 0{\cdot}159$; ——, $\hat{x}_s = 0{\cdot}174$; – – –, $\hat{x}_s = 0{\cdot}184$.

neglected. The details of the second approximation and its application to this configuration are described elsewhere (Dang 1974; Dang & Norrie 1975).

5.2. *Results for pressure fluctuations*

From (7), the coefficient of net loading can be shown to be

$$C_p(\hat{x}_s) = -2 \sum_{m=-\infty}^{\infty} C_m(\hat{x}_s) \exp(imN\theta_s), \tag{86}$$

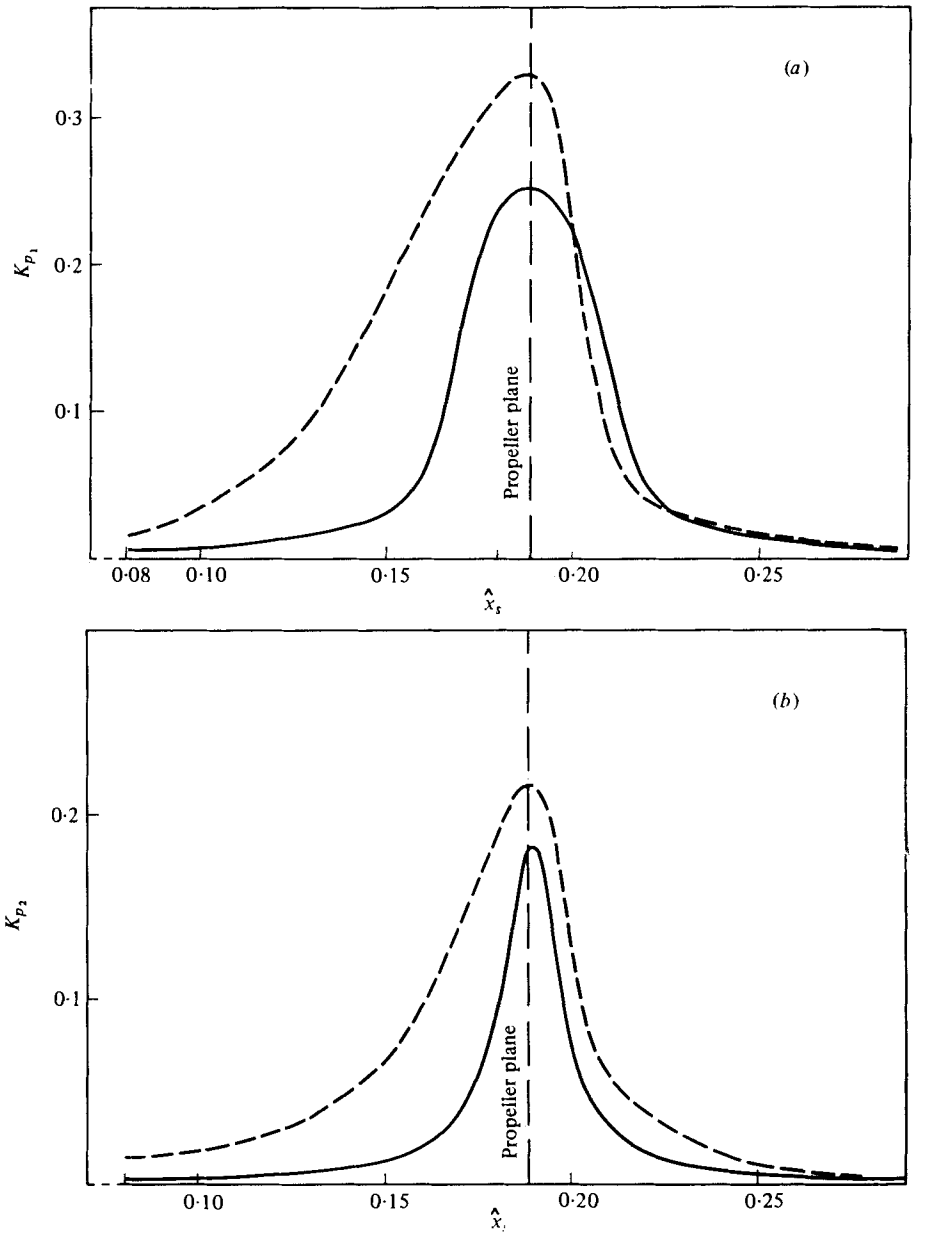

FIGURE 8. Coefficient of pressure K_{p_m}; $J_I = 0{\cdot}74$. (*a*) First harmonic. (*b*) Second harmonic. – – –, experiment (Hale); ——, present theory.

where the coefficient is defined in terms of the inner and outer duct wall pressures by

$$C_p(\hat{x}_s) = \frac{p_{\text{inner}}(\hat{x}_s) - p_{\text{outer}}(\hat{x}_s)}{\frac{1}{2}\rho U^2}. \tag{87}$$

For the zeroth harmonic the coefficient reduces to

$$C_{p0}(\hat{x}_s) = -B_0(\hat{x}_s), \tag{88}$$

and for the higher harmonics the net pressure coefficient becomes the inner wall

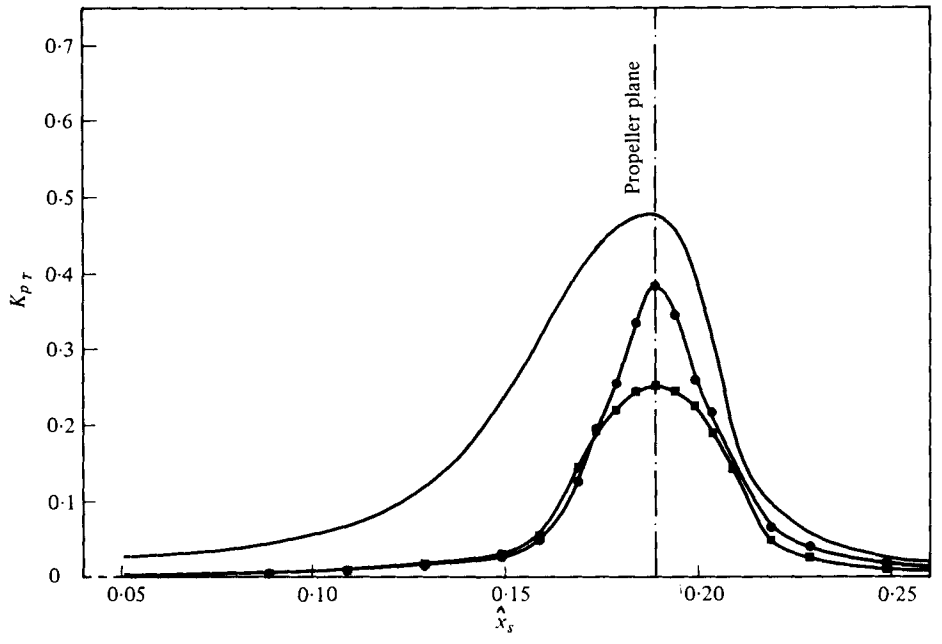

FIGURE 9. Coefficient of total pressure $K_{pT}(\hat{x}_s)$. ——, experiment (Hale); —●—, present theory (sum of two harmonics); —■—, present theory (one harmonic).

coefficient (since the Hale configuration has a long parallel duct outside which the pressure fluctuations can be assumed negligible)

$$C_{pm}(\hat{x}_s) = -2\{A_m(\hat{x}_s)\sin mN\theta_s + B_m(\hat{x}_s)\cos mN\theta_s\}. \tag{89}$$

The form used by Hale for the pressure field on the duct inner wall (Hale 1966; Hale & Norrie 1966; Norrie & Hale 1968) can be rewritten as

$$p = \sum_{m=-\infty}^{\infty} \alpha_m \exp[imN(\theta-\gamma)], \tag{90}$$

where
$$2\alpha_{\pm m} = \beta_m \mp i\gamma_m, \quad \beta_m = A_i\cos\epsilon_m, \quad \gamma_m = A_i\sin\epsilon_m \tag{91}$$

and the coefficient A_i is as defined by Hale (1966), Hale & Norrie (1966) and Norrie & Hale (1968). Comparison of (86) and (90) shows that the theoretical and experimental results are obtained in similar forms. The two pressure coefficients can be shown to be related by the expression

$$R_E \equiv C_{p\text{Hale}}/C_{p\text{present}} = \tfrac{1}{2}\pi^2 J^2\mu^2. \tag{92}$$

The results for A_m and B_m calculated from the theoretical analysis are shown in figures 6(*a*) and (*b*). Using these data, the net pressure coefficient was calculated from (89) and the results for several upstream positions are shown in figures 7(*a*) and (*b*). The results from the present analysis are plotted with Hale's data in the form of the net coefficient of harmonic pressure K_{p_m}† and net coefficient of total pressure K_{p_t} in figures 8 and 9.

For the first harmonic, downstream of the propeller and at a distance $\Delta\hat{x}_p > 0{\cdot}05R$ from the propeller plane, there is good agreement between the theoretical and experimental results for pressure fluctuations. For the second harmonic, the downstream

† Based on half the peak-to-peak amplitude.

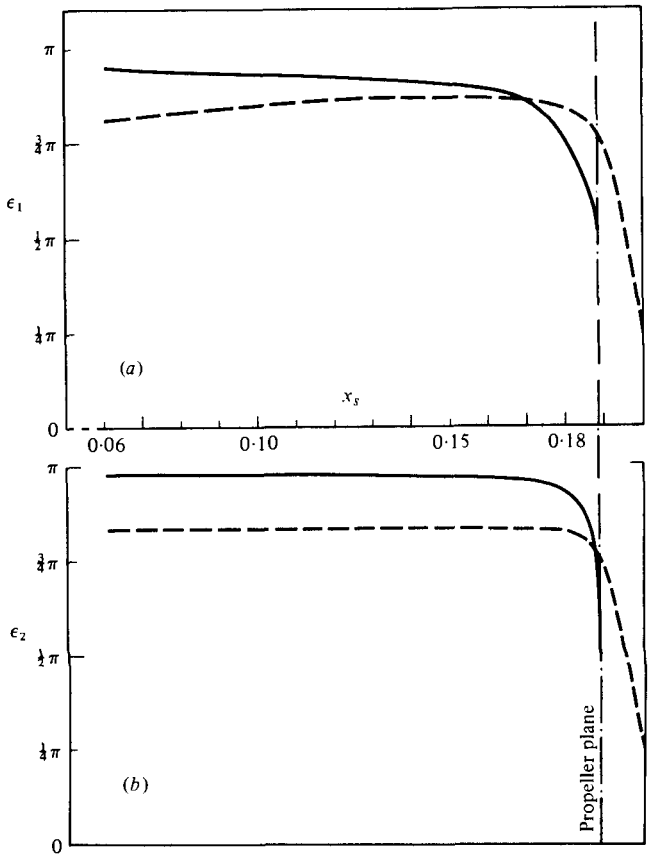

FIGURE 10. Comparison of theoretical and experimental phase angles $\epsilon_m(\hat{x}_s)$; upstream positions. (*a*) $m = 1$. (*b*) $m = 2$. ——, present theory; – – –, experiment (mean line).

results do not show quite such good correlation. The upstream results for theory and experiment, although of the same general form, show poor agreement.

As noted previously, close to the propeller the theoretical results would be expected to be in error because of the imperfection of the vortex-line model in representing the real system. The effect of blade vorticity being distributed along the chord as well as the effects of blade thickness and viscosity would be much more pronounced in this region than in the far field away from the propeller. The good agreement downstream of the propeller (except in the very near field) was to be expected because the approximate method of solution retained the dominant oscillating parts of the kernels and absolute terms in this region. Similarly, the poor correlation upstream might also have been expected because of the absence of oscillating parts upstream and the neglect of the singular and regular parts of the kernels in this region.

5.3. *Results for phase angles*

The series (90) used to represent Hale's pressure field on the inner duct surface can also be written as

$$p = \sum_{m=1}^{\infty} \alpha_m \cos\{4m(\theta - \gamma) + \epsilon_m\}, \tag{93}$$

where α_m is the modulus of the mth harmonic of the blade frequency pressure, ϵ_m is the angle by which the mth harmonic leads the propeller-blade position, θ is the propeller-blade angle and γ is the angular position of the point being considered. The phase angle ϵ_m can be calculated from the theoretical results using (42) for comparison with Hale's experimental data.

In figure 10 the calculated phase-angle data are presented together with Hale's experimental results, for harmonics $m = 1, 2$. Only the upstream results are shown since the downstream experimental data were too scattered to allow a meaningful comparison. The good agreement between theoretical and experimental phase angles evident in figure 10 upstream of the propeller requires some explanation in view of the relatively poor correlation shown between upstream pressure amplitudes. Examination of (89) shows (on dividing by B_m) that the phase angle ϵ_m depends on the ratio A_m/B_m whereas the pressure amplitude depends on A_m and B_m separately. It would appear that the neglect of the regular and singular parts of the kernels does not significantly affect the ratio A_m/B_m upstream (at least for the Hale configuration), thus allowing the phase angle ϵ_m still to be predicted with good accuracy. The changes in A_m and B_m separately due to the approximation, however, are apparently sufficient to put the pressure amplitude considerably in error upstream.

The research described in this paper was financially supported by the University of Calgary (Dissertation Fellowship), the Defence Research Board of Canada (Grant No. 9550–32) and the National Research Council of Canada (Grant No. A4192).

REFERENCES

BURNELL, J. A. & SACKS, A. H. 1962 Ducted propellers – a critical review of the state of the art. *Prog. Aero. Sci.* **3**, 85–135.

DANG, D. Q. 1972 A perturbation method for the solution of singular integral equations. *Univ. Calgary, Mech. Engng Dept. Rep.* no. 36.

DANG, D. Q. 1973 The calculation of a certain class of Fourier integrals. *Univ. Calgary, Mech. Engng Dept. Rep.* no. 43.

DANG, D. Q. 1975*a* Fluctuating pressure field of a ducted propeller. Ph.D. thesis, Mech. Engng Dept., University of Calgary.

DANG, D. Q. 1975*b* General solution of singular integral equations. *Univ. Calgary, Mech. Engng Dept. Rep.* no. 67.

DANG, D. Q. & NORRIE, D. H. 1975 The fluctuating pressure field of a ducted impeller. *Univ. Calgary, Mech. Engng Dept. Rep.* no. 66.

HALE, M. R. 1966 Hydrojet ducted propulsion system – impeller induced vibratory pressures and performance characteristics. Ph.D. thesis, Mech. Engng Dept., University of Adelaide.

HALE, M. R. & NORRIE, D. H. 1966 Hydrojet ducted propulsion system – impeller induced vibratory pressures and performance characteristics. *Univ. Adelaide, Mech. Engng Dept. Rep.* no. R66/3.

MORGAN, W. G. & CASTER, E. B. 1968 Comparison of theory and experiment on ducted propellers. *Proc. 7th Symp. Naval Hydrodyn.*

NORRIE, D. H. & HALE, M. R. 1968 The fluctuating pressure field of a ducted impeller. *Proc. A.S.M.E. Symp. Pumping Machinery for Marine Propulsion, Philadelphia.*

ORDWAY, D. E. & GREENBERG, M. D. 1961 General harmonic solutions for the ducted propeller. *Therm. Adv. Res., Ithaca, Rep.* TAR-TR 613.

ORDWAY, D. E., SLUYTER, M. M. & SONNERUP, B. O. U. 1960 Three dimensional theory of ducted impellers. *Therm. Adv. Res., Ithaca, Rep.* TAR–TR 602.

WEISSINGER, J. & MAASS, D. 1968 The theory of the ducted propeller – a review. *Proc. 7th Symp. Naval Hydrodyn.*